BRNO UNIVERSITY OF TECHNOLOGY
VYSOKÉ UČENÍ TECHNICKÉ V BRNĚ

CENTRAL EUROPEAN INSTITUTE OF TECHNOLOGY
STŘEDOEVROPSKÝ TECHNOLOGICKÝ INSTITUT

X-RAY NANO COMPUTED TOMOGRAPHY OF STRUCTURED POLYMERIC BIOMATERIALS
RENTGENOVÁ POČÍTAČOVÁ NANO TOMOGRAFIE POLYMERNÍCH STRUKTUROVANÝCH BIO MATERIÁLŮ

DOCTORAL THESIS SUMMARY
TEZE DIZERTAČNÍ PRÁCE

AUTHOR
AUTOR PRÁCE

Ing. Dominika Kalasová

SUPERVISOR
VEDOUCÍ PRÁCE

prof. Ing. Jozef Kaiser, Ph.D.

BRNO 2019

Summary

This thesis is focused on an advanced imaging method X-ray computed nanotomography (CT). This non-destructive technique is used for the research of various biomaterials in tissue engineering and material science in general (scaffolds, polymers, ceramics, composites, etc.). Visualisation and quantification in 3D are advantageous in multidisciplinary approach usually applied in these fields. The objective of the thesis is divided into two topics. The first topic is about optimisation of the measurement procedure for various soft materials by CT with the laboratory X-ray sources. Mostly, the phase contrast propagation-based CT imaging (PBI) is involved here. This work theoretically describes the PBI and demonstrates this phenomenon via several sets of measurements. The necessary post-processing of PBI data is implemented and evaluated based on data quality enhancement. The second topic shows specific applications of CT in material engineering. Several studies with different CT devices show a few examples of possible applications and image processing options. Examples of correlation of CT with other complementary techniques show how CT can be applied in a multidisciplinary approach to solving complex scientific problems.

Abstrakt

Tato práce se zaměřuje na pokročilou zobrazovací technologii, rentgenovou počítačovou tomografii (CT). Tato nedestruktivní technika je využívána pro výzkum různých biomateiálů ve tkáňovém inženýrství a materiálové vědě obecně (skafoldy, polymery, keramické materiály, kompozity aj.). Vizualizace a kvantifikace ve 3D jsou výhodné v rámci multidisciplinárního přístupu, který je často v těchto odvětvích uplatňován. Záměr této práce lze rozdělit do dvou oblastí. Prvním tématem je optimalizace měřicí procedury různých měkkých materiálů pomocí CT s laboratorními rentgenovými zdroji. To zahrnuje převážně zobrazování ve fázovém kontrastu, konkrétně metodu volného šíření záření (VŠZ). Tato práce teoreticky popisuje VŠZ a demonstruje tento jev na řadě experimentů. Následné nezbytné zpracování dat získaných VŠZ je implementováno a vyhodnoceno na základě míry zlepšení obrazových dat. Druhé téma ukazuje konkrétní aplikace CT v materiálovém inženýrství. Několik studií s různými CT zařízeními ukazuje příklady možných aplikací a obrazového zpracování. Příklady korelace CT dat s jinými doplňkovými technikami ukazují, jak může být CT aplikována v multioborovém přístupu ke komplexnímu řešení vědeckých problémů.

Keywords

X-ray computed tomography, nanotomography, nCT, phase contrast, phase retrieval, polymers, biomaterials

Klíčová slova

rentgenová počítačová tomografie, nanotomografie, nCT, fázový kontrast, polymery, biomateriály

Rozšířený abstrakt

Tato práce se zaměřuje na pokročilou zobrazovací technologii, rentgenovou počítačovou tomografii (CT). Tato nedestruktivní technika je využívána pro výzkum různých biomateiálů ve tkáňovém inženýrství a materiálové vědě obecně (skafoldy, polymery, keramické materiály, kompozity aj.). Vizualizace a kvantifikace ve 3D pomocí CT jsou výhodné v rámci multidisciplinárního přístupu, který je často v těchto odvětvích uplatňován.

Záměr této práce lze rozdělit do dvou oblastí. Prvním tématem je optimalizace měřicí procedury měkkých materiálů pomocí CT zařízení s laboratorními rentgenovými zdroji. To zahrnuje převážně zobrazování ve fázovém kontrastu, konkrétně metodu volného šíření záření (VŠZ). V této práci je popsán princip VŠZ a uvedené vztahy jsou aplikovány na popis jednotlivých CT zařízení. Na základě jejich analýzy jsou CT zařízení hodnocena z hlediska možností využití VŠZ. Jev je demonstrován na řadě experimentů měření polymerového kompozitu za různých nastavení přístroje. Následné nezbytné zpracování dat získaných VŠZ ve formě tzv. algoritmů pro získání fáze je implementováno a vyhodnoceno na základě míry zlepšení obrazových dat. Byl navržen software pro implementaci několika těchto algoritmů v případě CT zařízení RIGAKU nano3DX. Tento software bude implementován do oficiálního software firmy.

Druhé téma představuje některé konkrétní aplikace CT v materiálovém inženýrství. Několik studií s různými CT zařízeními ukazuje příklady možných využití VŠZ pro biomateriály a obrazovou analýzu dat. Jednou z aplikací je zobrazování buněk ve skafoldech. Je ukázáno zobrazení jak jednotlivých buněk s velkým rozlišením, tak i většího množství materiálu, což umožňuje celkové zhodnocení většího objemu vzorku. Druhým příkladem je analýza pórovitosti hydroxyapatitové pěny. Příklady korelace CT dat s jinými doplňkovými technikami ukazují, jak může být CT aplikována v multioborovém přístupu ke komplexnímu řešení vědeckých problémů. Je ukázána kombinace CT, skenovacího elektronového mikroskopu a světelné mikroskopie na vzorku skafoldu a kombinace CT, 3D energiově disperzní spektroskopie a světelné mikroskopie na vzorku vápence.

Konkrétním přínosem práce je rozšíření expertízy Laboratoře rentgenové počítačové tomografie na CEITEC VUT v oblasti zobrazování ve fázovém kontrastu. Implementace této metody na konkrétních tématech z materiálových věd rozšiřuje možnosti charakterizace především materiálů složených z lehkých prvků. Obecně tato práce přispívá k zavedení rentgenové počítačové tomografie jako běžné techniky k 3D zobrazování a analýze biologických vzorků. Nejdůležitější výsledky práce jsou autorkou publikovány v odborných impaktovaných časopisech a byly prezentovány na mezinárodních konferencích.

Contents

Introduction

X-ray computed tomography (CT) is a nondestructive method for imaging of materials. In principle, it acquires 3D information about the sample via a set of X-ray projections under different angles of a sample's rotation. In such a CT scan, an inner structure of an object is visualised. Based on the different response of materials to X-rays, an absorption or phase contrast can be measured or derived from the X-ray projections. In CT data, it is possible to get a slice through an object in an arbitrary direction. Various materials and structures can be distinguished, segmented and further analysed. Apart from visualisation, a number of useful information can be derived – size, volume, surface, 3D distribution, porosity, etc., and a variety of analyses including dimensional measurements and modelling of physical properties can be performed.

Many fields of science and industry take advantages of CT. The main features used by industry follow the quality control – dimensional measurements of otherwise inaccessible parts, comparison of manufactured parts to a CAD model, control of geometrical tolerances, various analyses of porosity, fibre orientation and wall thickness, etc. Some of them are also used in the science field. In the case of biomaterials, the challenge of segmentation, e.g. of determination of surface/border of different materials, is often more difficult than in industry. The reason is that those materials contain a lot of various structures, which may have similar or low contrast to be distinguished easily. Often, some a priori knowledge about the sample is needed. The purpose of the further analysis is often case-dependent and requires the development of specific post-processing procedures, usage of specialised CT software or utilisation of advanced programming methods.

Obtaining CT data of structures from biomaterials and establishing a meaningful post-processing method is a challenging task. They are composed of light materials with low X-ray absorption and/or contrast, which makes use of absorption CT used in industry difficult or even impossible. This can be overcome by staining of the sample with heavier elements or by use of phase contrast imaging methods. The latter requires careful mathematical post-processing of X-ray projections to get meaningful data. Once the CT data are acquired, and the desired structures are visible, the segmentation and quantification bring another challenge for both CT-devoted software and programmers working with image analysis. To get a reliable interpretation of CT data, often additional 2D/3D imaging methods are required to complement CT results and to establish the technique in the framework of currently used methods.

The chapter "Literature review" is not included in this doctoral thesis summary. The following chapter, here the first one, sums up the aims of the thesis. In the second chapter, the CT devices, software and image evaluation tools used in the thesis are described.

The next two chapters form the main content of the thesis. The third chapter explores the propagation-based method of phase contrast imaging with laboratory-based X-ray

sources from the theoretical and experimental point of view. It includes characterisation of two laboratory-based CT systems for propagation-based imaging (PBI), implementation and optimisation of phase retrieval algorithms and optimisation of measurement parameters for PBI. In chapter four, examples of phase contrast imaging and subsequent post-processing of light materials are shown. The most important results from the fourth and fifth chapter are published in impacted journals. Some of the results were presented at international conferences.

1. Aims of thesis

The general aim of this thesis is to study, explore and bring new insights into the field of imaging of polymer biomaterials by X-ray computed nanotomography. This is achieved by the exploration of two areas of interest: research and development of CT imaging itself, specifically propagation-based phase contrast imaging, and application of this technique on specific applications in material science.

1.1. Propagation-based phase contrast imaging

CT imaging of light materials like polymers and soft tissues is not as easy and straight-forward as imaging of heavy, metal samples from industry, geology, and similar. These materials often do not have sufficient X-ray absorption and/or contrast in X-ray region. The problem of CT imaging of such samples is, in general, solved by staining to increase contrast or by use of specific imaging methods like phase contrast imaging.

The goal here is to explore phase contrast imaging with laboratory-based CT devices. Experiments optimising the propagation-based imaging (PBI) procedures will be designed, performed and evaluated. Results of this technique from several CT machines will be shown, including the work from the author's internships abroad.

Special focus will be on the post-processing of data acquired via PBI. This includes mainly the implementation of phase retrieval algorithms. A simple tool for easy testing and application of phase retrieval will be developed specifically for the needs of the Laboratory of X-ray computed micro and nanotomography at CEITEC BUT. Also, the influence of phase retrieval on data quality in dependence on measurement parameters will be studied.

1.2. Applications on biomaterials

Among other methods of material's imaging, the CT technique is distinguished by the possibility of studying the whole sample without its destruction and in 3D. A lot of information of interest can be derived from CT data (morphology characteristics, pore analysis, etc.) Nevertheless, it is often advantageous to complement CT data with other, quantitative technique since a basic CT measurement cannot determine the composition of the sample.

Several case-studies of CT imaging of various biomaterials (scaffolds, foams, ...) will be shown. They include phase contrast imaging and a few image analysis procedures. They may be done in VG Studio MAX software, Matlab, ImageJ or any other convenient tool. Another task in the thesis is a combination of CT data with other 2D or 3D analysing

and imaging methods, such as optical or electron microscopy, serial sectioning etc. Two studies presenting such correlation will be shown.

2. Methods

2.1. CT devices

In this section, the CT devices used for experiments in this doctoral thesis topic are described: RIGAKU nano3DX, GE phoenix v|tome|x L240 and Thermo Fisher Scientific HeliScan located at the Brno University of Technology, and Zeiss Xradia nanoXCT-100 located at the University of Jyväskylä in Finland (Fig. 2.1). Technical details and specifications regarding sample preparation and imaging are included. The following shortcuts are used: LPS – linear pixel size, LVS – linear voxel size, FOV – field of view.

Figure 2.1: CT machines used in the thesis: a) RIGAKU nano3DX, b) Thermo Fisher Scientific HeliScan, c) GE phoenix v|tome|x L240, d) Zeiss Xradia nanoXCT-100.

2. METHODS

RIGAKU nano3DX

Most of the measurements are performed with CT device RIGAKU nano3DX, located at the Central European Institute of Technology, Brno University of Technology (Fig. 2.1a). Sample–source distance is relatively large (≈ 260 mm) compared to the typical sample size (few mm), so the beam is considered semi-parallel at the sample stage.

The X-ray source is the RIGAKU rotating anode with three target materials available (Cu (40 kV tube voltage, 30 mA tube current), Mo (50 kV, 24 mA), and Cr (35 kV, 25 mA)). The focal spot size is 73 μm for Cu and 156 μm for Mo target measured according to the EN 12543-5 norm.

Experiments in the thesis are performed with two different types of X-ray cameras, CCD (charge-coupled device) and sCMOS (scientific complementary metal-oxide-semiconductor). The camera consists of a scintillator, magnification optics and a detector. Several optical units with different magnifications can be used to reach different effective LPS and FOV (for the smallest optical unit for CCD camera: LPS 0.27 μm, FOV 0.7×0.9 mm^2).

CT measurements can be performed either in Continuous mode (the sample is continuously rotating during the measurement) or Step mode (the sample does not move during the acquisition of a projection). The typical scanning times are 1–3 hours. According to the author's experience, it is necessary to prepare the sample in advance and to let it temperate in the sample chamber for at least several hours to avoid sample movement due to thermal expansion.

Thermo Fisher Scientific HeliScan

Thermo Fisher Scientific HeliScan CT device is located at the Central European Institute of Technology, Brno University of Technology (Fig. 2.1b). The system is equipped with micro-focus X-ray source with 8 W power with up to 160 kV voltage. The target material is tungsten. The focal spot size varies between 0.8 μm and 4 μm according to the applied settings (it is possible to choose from three different spot sizes in this range). The geometry of the system allows to set maximum source–sample distance 130 mm and maximum source–detector distance 750 mm. The detector is a large area 16-bit detector with 3072×3072 pixels with 139 μm pixel size. When performing CT measurements, several scanning trajectories are available: circular and helical ones – single helix, double helix and space filling.

GE phoenix v|tome|x L240

CT device GE phoenix v|tome|x L240,, located at the Central European Institute of Technology, Brno University of Technology (Fig. 2.1c), was used for an application study. This large microCT system is placed in an air-conditioned cabinet. All components are on the granite-based 7-axis manipulator for long-term stability. The system has a cone beam geometry. The samples up to 500×800 mm^3 and 50 kg can be scanned. The machine is equipped with a GE DXR 250 flat panel detector.

Zeiss Xradia nanoXCT-100

CT device Zeiss Xradia nanoXCT-100, located at the University of Jyväskylä in Finland (Fig. 2.1d), was used for an application study. Images were taken during 4-months Erasmus internship at this university from February to May 2018. With this machine, two imaging modes are available: absorption (without the phase ring) and phase contrast mode (with the phase ring). Rotating RIGAKU Cu anode (40 keV, 30 mA) emerges X-rays from 70 μm focal spot. Two imaging modes are available: "Large field of view", LFoV (LVS 65 nm, FOV $60 \times 60\,\mu m^2$), and "High resolution", HiRes (LVS 10 nm, FOV $15 \times 15\,\mu m^2$).

The schematic diagram of the machine is in Fig. 2.2. A condenser capillary lens is installed to capture the X-rays and to focus them on the sample. To obtain a single focal spot, a pinhole is inserted just before the sample to isolate only the first order reflected X-rays. Fresnel zone plate is used as an objective. Optional phase ring is used to form a negative Zernike phase contrast. To reduce the loss of throughput, X-rays pass through flight tube filled with He gas. The detector consists of two magnifying lenses with scintillators (for alignment and imaging). X-rays converted to light are captured on a CCD camera.
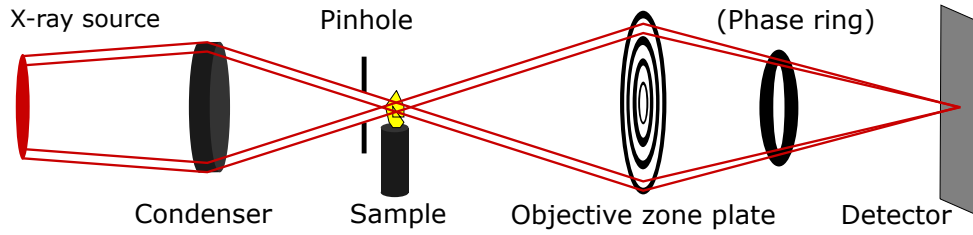
Figure 2.2: Xradia Zeiss nanoXCT-100 setup.

The whole system is very sensitive to the geometrical alignment of all components because X-rays are focused on a small spot on the sample. To reach optimal data quality, scanning times can be as high as several days. The final resolution is higher than the precision of mechanics of the sample stage. To overcome this difficulty, for every measurement, a gold microparticle has to be inserted into the sample. It is also used later for alignment of projections.

Since the field of view is very small, additional tools have to be used for sample preparation. For manipulation with the sample and the needle, micro-manipulators Sensapex SMX and micro-grippers SmarAct are used. The preparation is observed via a Leica Z16 APO microscope. If needed, the sample can be cut via laser on a QuikLaze CMPS-888L machine.

2.2. Software

The following software for data processing was used during work on this thesis (Tab. 2.1).

Table 2.1: List of software used in this thesis for data analysis.

	Fiji open source [1, 2]
	MATLAB MathWorks, USA [3]
	VGStudio MAX Volume Graphics, Germany [4]
	MAVI Fraunhofer Institute for Industrial Mathematics, Germany [5]
	Pore3D open source software for commercial IDL [6]

2.3. Image evaluation parameters

Several parameters for image evaluation are introduced in Fig. 2.3. Let I_{MAT} and I_{BCG} be the averaged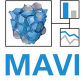 grey value intensities from areas inside sample material and in the background, respectively. If a line profile is generated[1], I_{MAT} and I_{BCG} correspond to the intensities at the ends of the line[2]. $I_{20\%}$ and $I_{80\%}$ correspond to 20 % and 80 % of the intensity difference between I_{MAT} and I_{BCG}. $x_{20\%}$ and $x_{80\%}$ correspond to the horizontal axis value of $I_{20\%}$ and $I_{80\%}$, respectively. I_{MAX} and I_{MIN} are the maximum and minimum values in the line profile, respectively.

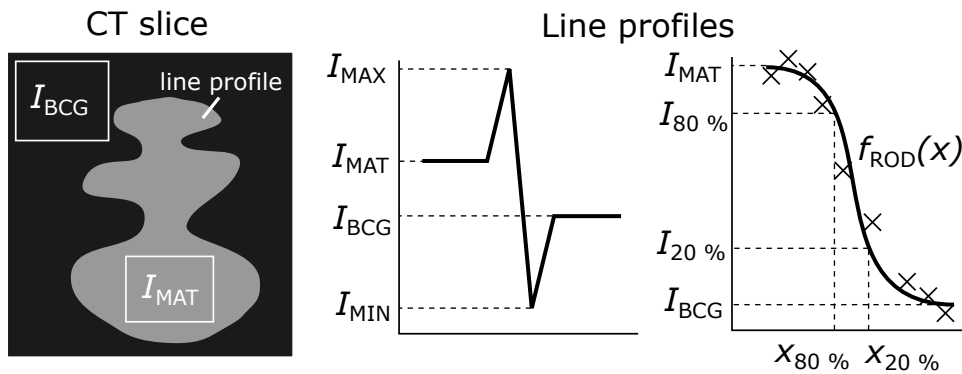Figure 2.3: Variables used in image evaluation parameters.

---

[1]Usually, several pixels above and below the line are averaged to reduce the noise.
[2]Usually, several utmost pixels are averaged to reduce the noise.

Parameters based on information from selected area

- Histogram. Graphical representation of grey values distribution in a given area (typically a CT slice).

- Signal to noise ratio SNR[3].
$$\text{SNR} = \frac{I_{\text{MAT}}}{\text{std}\, I_{\text{BCG}}}$$

- Signal to noise ratio gain SNR_{gain}

$$\text{SNR} = \frac{\text{SNR(phase retrieved image)}}{\text{SNR(original image)}}$$

Parameters based on line profile

- Absorption contrast C_{ABS}

$$C_{\text{ABS}} = \frac{I_{\text{MAT}} - I_{\text{BCG}}}{(I_{\text{MAT}} - I_{\text{BCG}})/2}$$

- Absorption contrast gain $C_{\text{ABS, gain}}$

$$C_{\text{ABS, gain}} = \frac{C_{\text{ABS}}(\text{phase retrieved image})}{C_{\text{ABS}}(\text{original image})}$$

- Phase contrast C_{PHC}

$$C_{\text{PHC}} = \frac{I_{\text{MAX}} - I_{\text{MIN}} - (I_{\text{MAT}} - I_{\text{BCG}})}{I_{\text{MAX}} + I_{\text{MIN}}}$$

- Let f_{ROD} be the Rodbard function fitted to line profile with parameters a, b.

$$f_{\text{ROD}}(x) = I_{\text{BCG}} + \frac{I_{\text{MAT}} - I_{\text{BCG}}}{1 + (\frac{x}{b})^a}$$

  – Edge resolution R_{E}
$$R_{\text{E}} = |x_{20\%} - x_{80\%}|$$

  – Standard deviation of fitting of Rodbard function STD_{ROD}

$$\text{STD}_{\text{ROD}} = \sqrt{\frac{\sum_i^N [I(x_i) - f_{\text{ROD}}(x_i)]^2}{N}}$$

---

[3]std x means standard deviation of x.

2. METHODS

3. Propagation-based imaging

Only a limited number of images and results is included in this doctoral thesis summary.

3.1. Characterization of lab-CT systems for PBI

With knowledge of parameters of a CT machine, it is possible to estimate suitability of the device for propagation-based imaging based on criteria explained in the full version of the thesis. Two CT machines (RIGAKU nano3DX (Sec. 2.1) and Thermo Fisher Scientific HeliScan (Sec. 2.1)) are described and discussed in terms of PBI. Calculations are supplemented with measurements of polymeric samples.

3.1.1. PBI on nano3DX

The study was published by the author of the thesis in [7], titled "Characterization of a laboratory-based X-ray computed nanotomography system for propagation-based method of phase contrast imaging".

Abstract

"Phase-contrast imaging (PCI) is used to extend X-ray computed nanotomography (nCT) technique for analyzing samples with a low X-ray contrast, such as polymeric structures or soft tissues. Although this technique is used in many variations at synchrotrons, along with the recent development of X-ray tubes and X-ray detectors, a phase contrast imaging becomes available also for laboratory systems.

This work is focused on determining the conditions for propagation-based PCI in laboratory nCT systems based on three criteria. It is mostly employed in near-field imaging regime, which is quantified via Fresnel number. X-rays must reach certain degree of coherence to form edge-enhancement. Finally, setup of every CT measurement has to avoid geometrical unsharpness due to the finite focal spot size. These conditions are evaluated and discussed in terms of different properties and settings of CT machine. Propagation-based PCI is tested on a sample of carbon fibres reinforced polyethylene and the implementation of Paganin phase retrieval algorithm on the CT data is shown." [7]

3.1.2. PBI on HeliScan

A study similar to the evaluation of PBI on RIGAKU nano3DX (Sec. 3.1.1) was also carried out with CT device Thermo Fisher HeliScan. The preliminary results were presented by the author of this thesis at the International Conference on Tomography of Materials and Structures in Cairns, Australia, on July 2019. Up to the date of submitting of this thesis, the experimental results are still under evaluation, and they are planned to be published in an impacted journal in autumn 2019 or winter 2020. Therefore here, only numerical evaluation is provided.

Theoretical estimation of PBI abilities of HeliScan includes evaluation of imaging regime represented by Fresnel number N_{F}, visibility of PBI effects related to a degree of X-ray coherence represented by $L_{\mathrm{shear}}/L_{\mathrm{lat}}$ ratio, and geometrical unsharpness due to finite focal spot size. In contrast to nano3DX, HeliScan offers more variability in terms of setting source–sample distance (denoted here as sample position y_{S}), source–detector distance (denoted here as y_{D}), X-ray tube voltage, and focal spot size. The calculations are made for two effective propagation distances, 5 mm and 10 mm. These two represent two measurement settings with different sample and detector positions and the same linear voxel size 2 μm (Tab 3.1). As a wavelength, the mean energy of spectra with acceleration voltage 50 kV generated by SpekCalc software [8] was used, unless stated otherwise.

Table 3.1: Two possible geometrical settings of Thermo Fisher HeliScan to reach different effective propagation distances.

Source–sample distance y_{S} [mm]	Source–detector distance y_{D} [mm]	Effective propagation distance z_{eff} [mm]
5	300	5
11	718	11

Dependence of the Fresnel number on the structural component of size a shows a quick increase to very high numbers ($\gg 1$) for both measurements (Fig. 3.1a). Thus, the imaging is in the near field regime for all recognizable features (considering the linear voxel size of 2 μm). The edge enhancement should be the most pronounced for small features of size about a few microns.

The imaging regime does not depend on focal spot size, but it can vary with the X-ray energy. The plot of N_{F} for different X-ray tube voltages (thus mean X-ray energy of the spectra) suggests that this parameter is not much significant for the imaging regime in the range of energies available for HeliScan (Fig. 3.1b).

Both sets of measurements have almost identical dependence of $L_{\mathrm{shear}}/L_{\mathrm{lat}}$ ratio on a (Fig. 3.2a). The differences are not visible on the displayed scale. However, the degree of coherence is influenced by the focal spot size (Fig. 3.2b). If the smaller spot size is used, the phase effects are better visible.

Distances of both the sample and the detector from the source can be varied. A user has to select them carefully to avoid geometrical unsharpness due to finite focal spot size. All possible pairs of y_{S} and y_{D} lay in the region restricted by lines in Fig. 3.3.

(a)   (b)

Figure 3.1: Fresnel number N_F dependence on structural component of size a. a) Plot for two sets of measurements with different effective propagation distances (Tab 3.1), b) plot for the spot size $0.8\,\mu$m, geometrical settings $y_S = 5\,$mm, $y_D = 300\,$mm, and for different X-ray tube voltages.

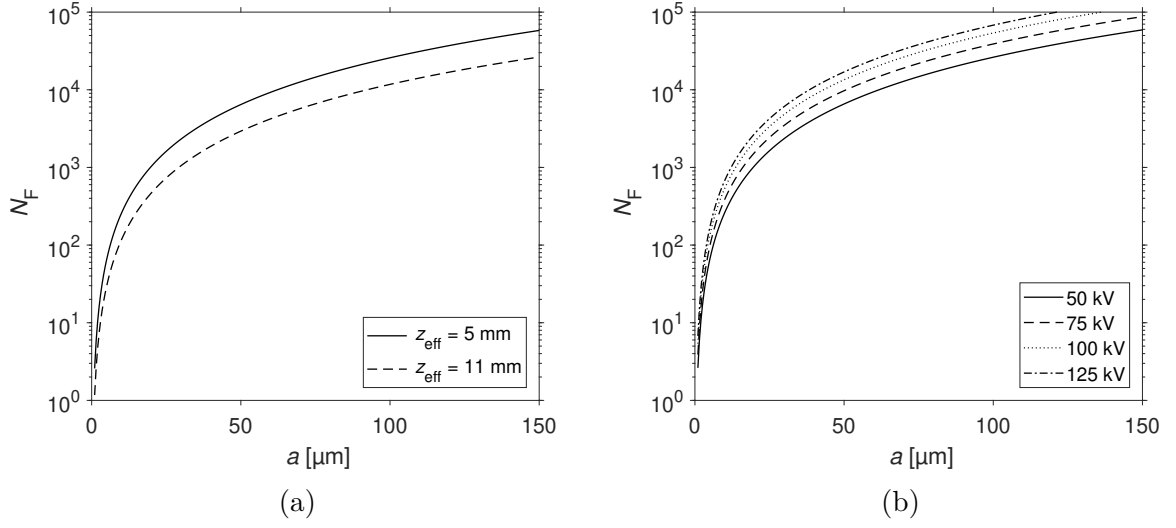(a)   (b)
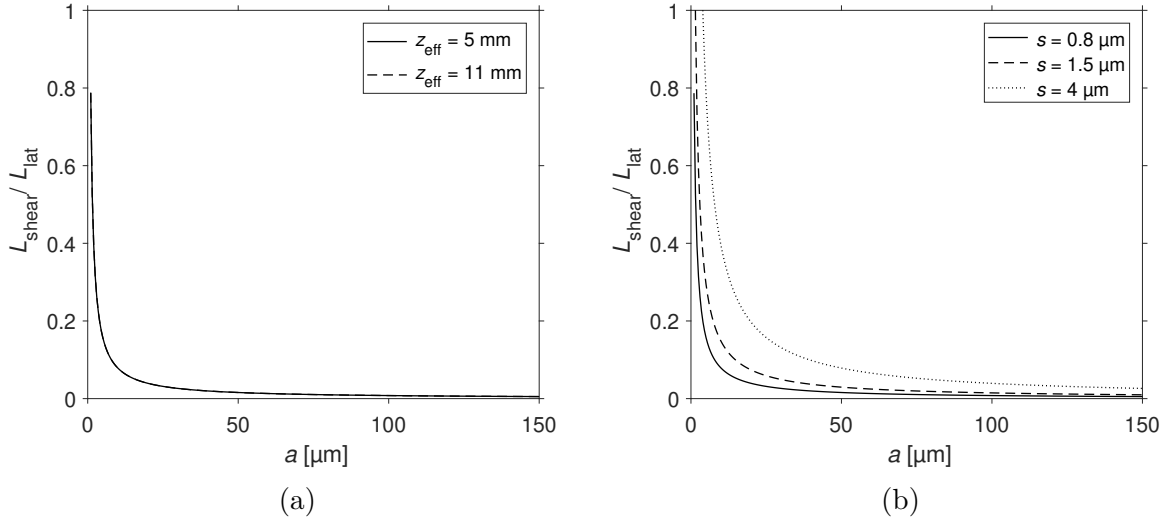
Figure 3.2: L_{shear}/L_{lat} dependence on structural component of size a. a) Plot for two sets of measurements with different effective propagation distances (Tab 3.1), b) plot for the X-tay tube voltage $50\,$kV, geometrical settings $y_S = 5\,$mm and $y_D = 300\,$mm and for different spot sizes.
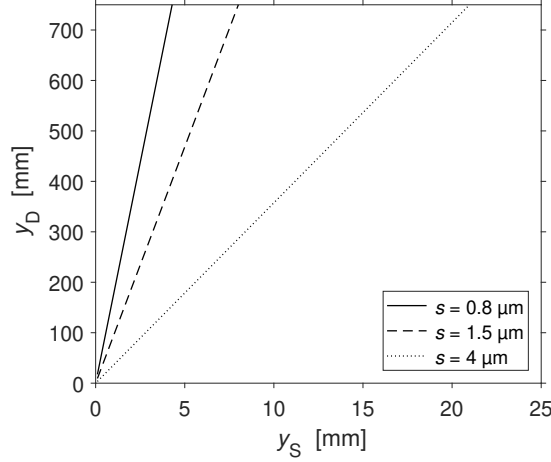
Figure 3.3: Maximum detector position y_D to avoid geometrical unsharpness for different spot sizes.

3.2. Phase retrieval implementation

3.2.1. Matlab GUI

During her internship in RIGAKU company (Tokyo, Japan) in autumn 2018, the author of the thesis studied propagation-based phase contrast imaging with the nCT system RIGAKU nano3DX. She created a graphical user interface (GUI) in Matlab [3] for application of phase retrieval on data from nano3DX. The program includes several algorithms (Paganin algorithm – PA, Modified Bronnikov Algorithm – MBA, Bronnikov Aided Correction – BAC). In practice, a sample usually contains several materials, so it is difficult to determine the exact physical value of parameters for phase retrieval. Therefore a test mode for choosing optimal parameters is included. Up to the date of submitting of this thesis, this GUI is being implemented into official RIGAKU software, and it will be provided to customers in 2020.

In the main window of the GUI (Fig. 3.4a), in the panel *Input files*, the user selects a .raw file containing projections. Data from the measurement from the .ctm file with the same name are loaded to generate the input parameters for phase retrieval (dimensions of the file, wavelength, sample–detector distance, pixel size). It is possible to go through the projections by the horizontal slider and select a slice for testing by the vertical slider.

In the panel *Choose mode*, a mode for testing (on a slice or an projection) or execution is selected. This choice enables one of the two panels. The *Execution mode setting* panel (Fig. 3.4b) is used for performing phase retrieval on the whole .raw file with user-defined parameters optimised in the *Test mode*. Phase-retrieved files called *…_phase_algorithm_-parameter.raw* and corresponding .ctm files are generated.

The panel *Test mode setting* is meant to find optimal algorithms and parameters for the phase retrieval in individual measurements. The software can save all combinations of interest as .tiff files or show them in another window (Fig. 3.4c). Phase retrievals are showed either on projections or slices, according to the choice in the *Test on* panel (if on slices, a user has to insert a correct centre of rotation). Before the window opens, a user is asked to select a line and a material and background area to evaluate image
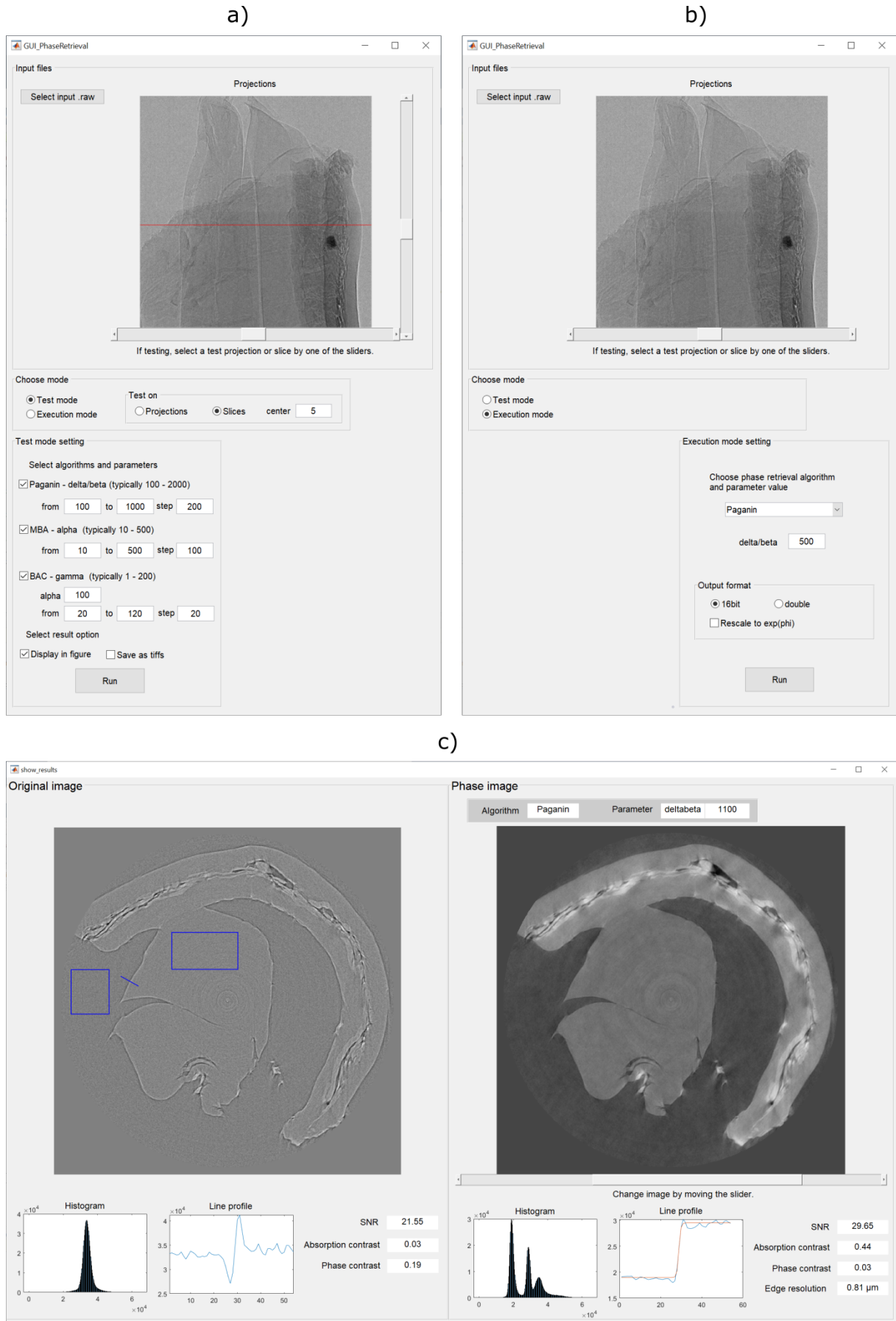
Figure 3.4: a)–c) graphical user interface in Matlab of a program, which implements phase retrieval on data from nano3DX.

quality. The window contains two panels, with the original and phase-retrieved images. In the latter, it is possible to move the slider to change the algorithms and parameters. For each image, a histogram and a line profile are shown. Image evaluation parameters SNR, absorption contrast, phase contrast and edge resolution, as they are introduced in Sec. 2.3, are shown.

3.2.2. Optimisation of phase retrieval parameters

Methodology

The influence of phase retrieval parameter on resulting data is studied on a sample of polyethylene rod with double-sided tape (PEDT) measured on nano3DX with sCMOS camera in the Continuous scanning mode for 15 min with Cu target, SDD 1.5 mm, bin 2, linear voxel size 0.64 μm and 600 projections. The sample consists of two polymers with slightly different density, which makes it a suitable sample for testing of PBI. The slice reconstructed without phase retrieval is in Fig. 3.5. Areas for image evaluation according to Sec. 2.3 are highlighted. The data were processed with phase retrieval, Paganin algorithm, for δ/β values from 100 to 2800.

Results

Slices and details or a selected area are presented in Fig. 3.7 together with corresponding histograms and line profiles. Several image evaluation parameters (Fig. 3.6) assess the influence of the choice of phase retrieval δ/β parameter to image quality.

When the δ/β value is set very low (close to 100 or lower), the image is very similar to the original image, as well as other characteristics. With increasing δ/β, the histogram becomes multi-modal, edge-enhancement disappears, SNR and C_{ABS} increase and C_{PHC} decreases. These improvements make the data look better, less noisy, and the segmentation of individual parts gets easier. On the other hand, the value of edge resolution R_{E} increases with increasing δ/β and some of the details in the structure can be lost. Overall blurring is visible in slices with δ/β above approximately 1500.

A closer look at the parameters can help to choose an optimal parameter for phase retrieval. SNR improvement is not linear with increasing δ/β and from some value, here about $\delta/\beta = 1000$, it starts to saturate. C_{PHC} does not decrease completely to 0, but there is a minimum about value $\delta/\beta = 1000$. This is related to the "sharpness" of the edge, which is described by $\mathrm{STD}_{\mathrm{ROD}}$. It has a minimum about the values 800–1000 as well.

Based on this thorough analysis, δ/β in the interval 800–1000 should be chosen to reach the optimal data quality with Paganin phase retrieval. It is slightly higher than the tabulated value for polyethylene, $\delta/\beta = 780$ [7, 9]. Using a similar analysis, it is possible to choose an optimal parameter for phase retrieval in the CT measurements.
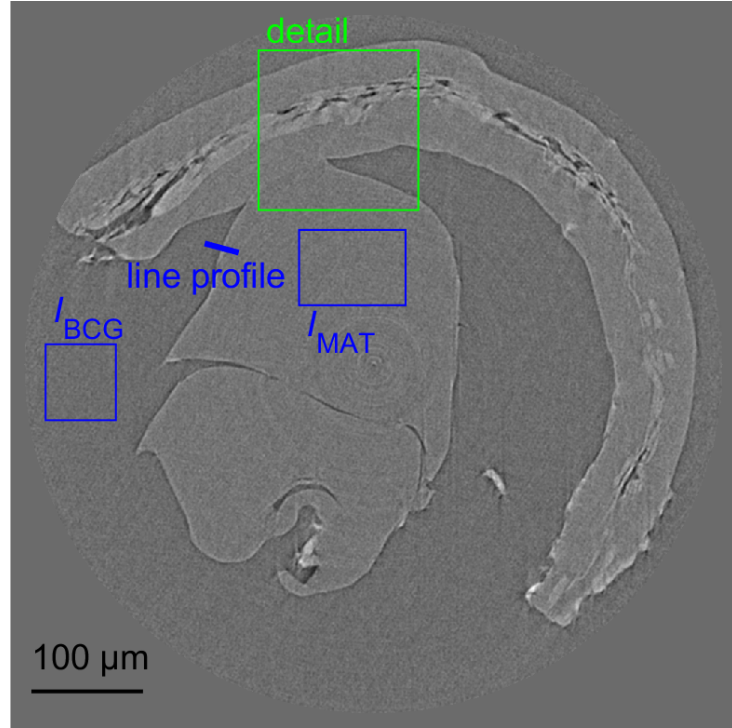
Figure 3.5: CT slice of the PEDT with highlighted areas for image evaluation.
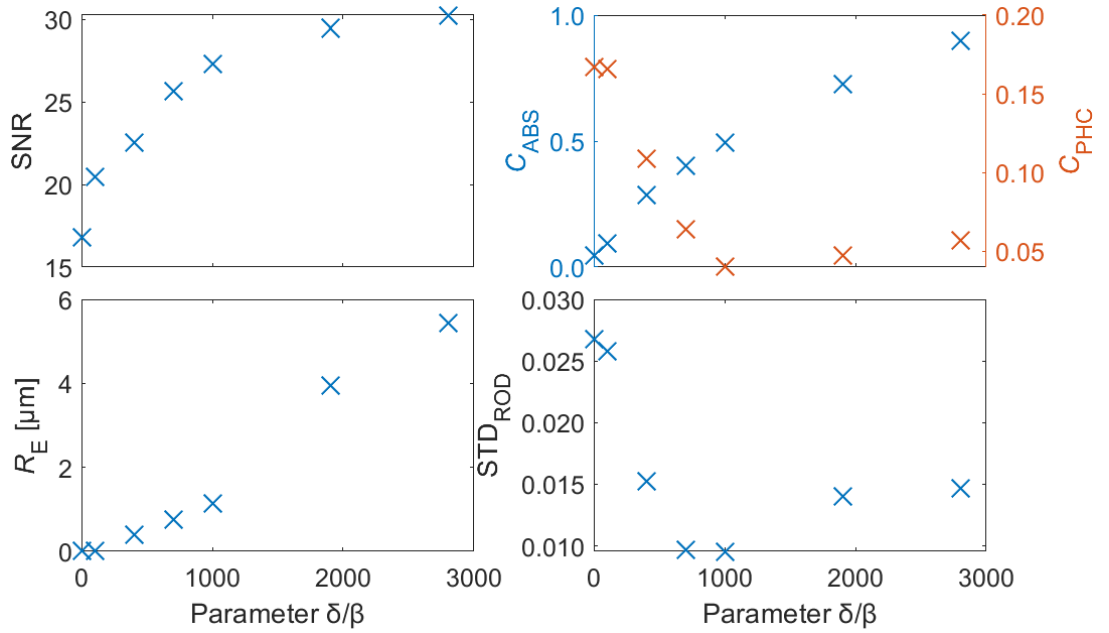
Figure 3.6: Dependence of various image evaluation parameters (Sec. 2.3) on δ/β value in phase retrieval (Paganin algorithm). The point $\delta/\beta = 0$ corresponds to data without phase retrieval. The data are shown in Fig. 3.7.
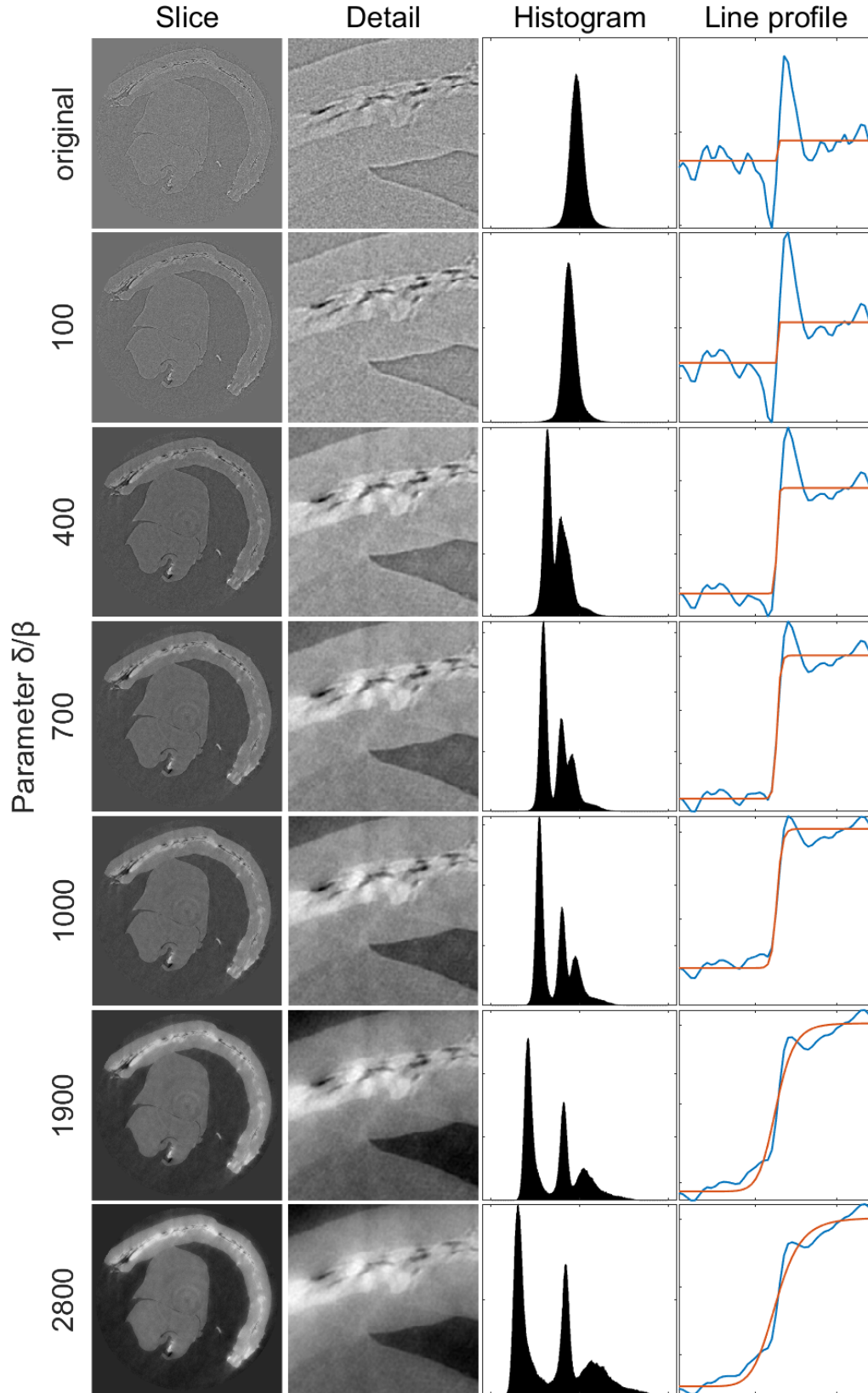
Figure 3.7: CT slices of the PEDT (first row). Paganin phase retrieval algorithm was applied with different δ/β values from 100 to 2800. For each image, a detail, a histogram and a line profile (blue) with fitted Rodbard function (orange) are shown in second, third and fourth column, respectively.

3.2.3. Comparison of phase retrieval algorithms

Methodology

The differences between four mostly used phase retrieval algorithms (Paganin algorithm – PA, Modified Bronnikov algorithm – MBA, Bronnikov aided correction – BAC) (Figs. 3.9, 3.10) are studied on a sample of polyethylene rod with double-sided tape (PEDT) measured on nano3DX with sCMOS camera in the Continuous scanning mode for 15 min with Cu target, SDD 1.5 mm, bin 2, linear voxel size 0.64 μm and 600 projections. The sample consists of two polymers with slightly different density, which makes it a suitable sample for testing of PBI. The slice reconstructed without phase retrieval with highlighted areas for image evaluation according to Sec. 2.3 is in Fig. 3.8.

Results

Slices processed with different algorithms (Figs. 3.9, 3.10) are accompanied with corresponding histograms (Fig. 3.11) and line profiles (Fig. 3.12). Several image evaluation parameters are calculated (Tab. 3.2) to discuss the influence of the algorithms on data.

The PA and MBA strongly reduce edge enhancement (in comparison with the original image, they have low values of C_{PHC}, STD_{ROD}, high values of C_{ABS}) and increase SNR. At the same time, the edge resolution gets worse for them as they filter out high frequencies. Indeed, in the detailed images, the PA and especially MBA are the most blurred images with some loss of detail. The BAC, on the other hand, preserves the details of the original image and increases C_{ABS} as well. However, the histogram shape has only one peak, which makes the segmentation difficult. The SNR increase is not as significant as in the case of PA.

The relatively worst performance of the MBA can be explained by the invalid assumption of a pure phase object since there is some X-ray absorption in the sample. Assumption of a single-material object with the PA is reasonably valid (all parts of the sample are similar polymers), hence the results are good and artefact-free. However, the BAC achieves the smallest loss of resolution compared to original data. The authors in [10] compared these algorithms on a sample of a spider stained with iodine and came up with a similar conclusion. To sum up, when one needs to focus on resolving the details of the structure, the BAC is recommended. If an easy segmentation and further post-processing is the priority, the PA is a good choice.

Table 3.2: Image evaluation parameters of CT slices of PEDT with different phase retrieval algorithms.

| Algorithm	SNR	C_{ABS}	C_{PHC}	R_E [μm]	STD_{ROD}
without	17	0.04	0.17	0.02	1754
Paganin algorithm	27	0.47	0.05	1.01	601
Modified Bronnikov alg.	30	0.27	0.08	0.73	775
Bronnikov aided correction	16	0.17	0.11	0.08	1083
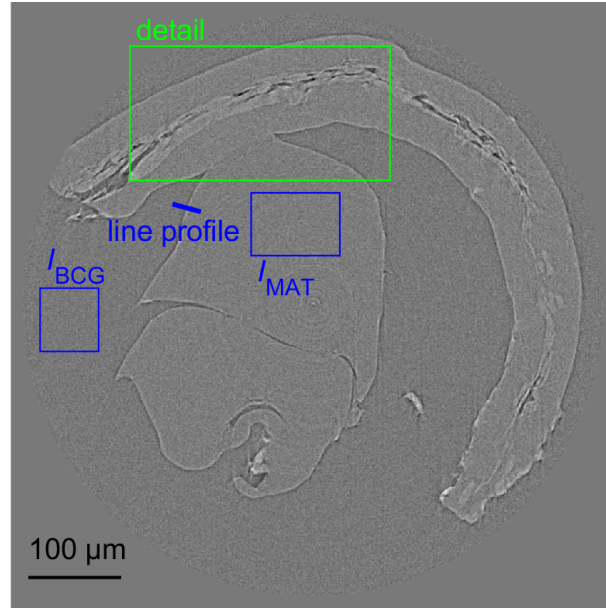
Figure 3.8: CT slice of the PEDT with highlighted areas for image evaluation.

Figure 3.9: CT slices of PEDT with different phase retrieval algorithms (Paganin algorithm – PA, Modified Bronnikov algorithm – MBA, Bronnikov aided correction – BAC).

Figure 3.10: Details of CT slices of PEDT with different phase retrieval algorithms (Paganin algorithm – PA, Modified Bronnikov algorithm – MBA, Bronnikov aided correction – BAC).

Figure 3.11: Histograms of CT slices of PEDT with different phase retrieval algorithms (Paganin algorithm – PA, Modified Bronnikov algorithm – MBA, Bronnikov aided correction – BAC).
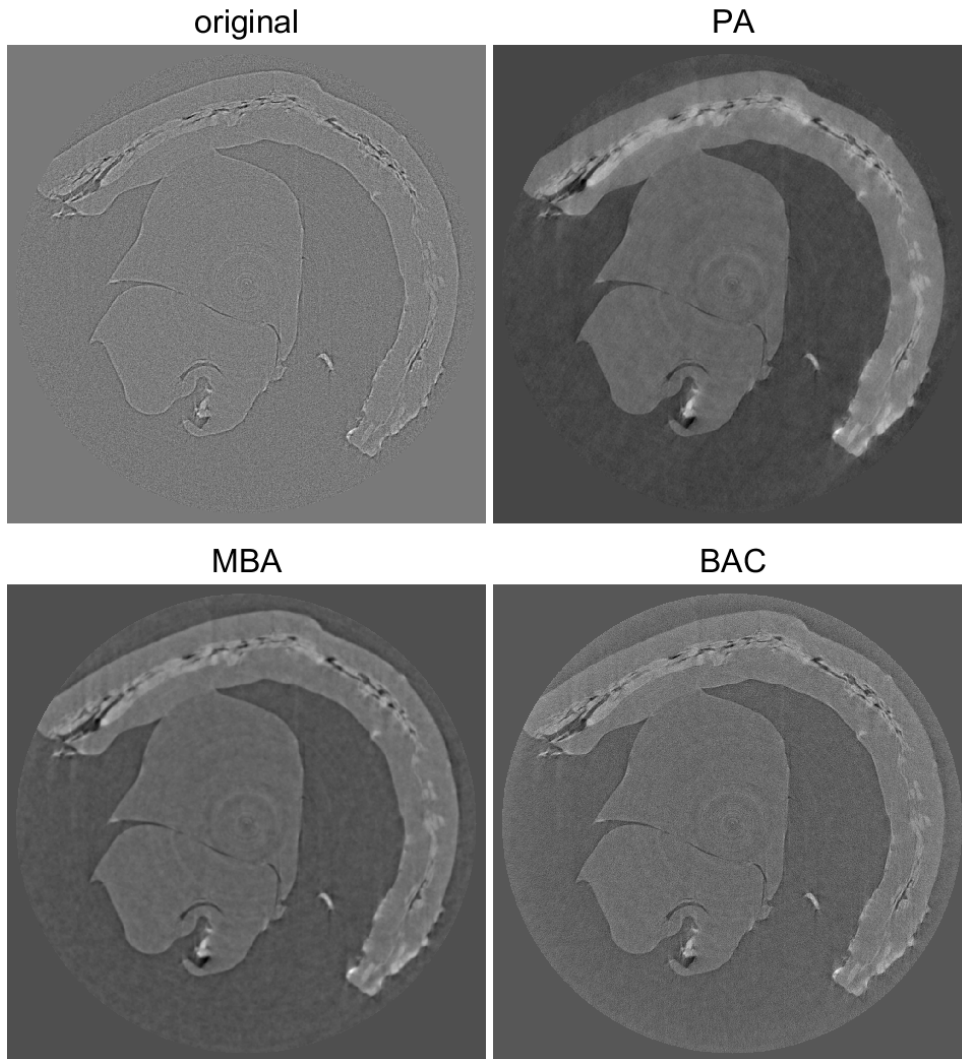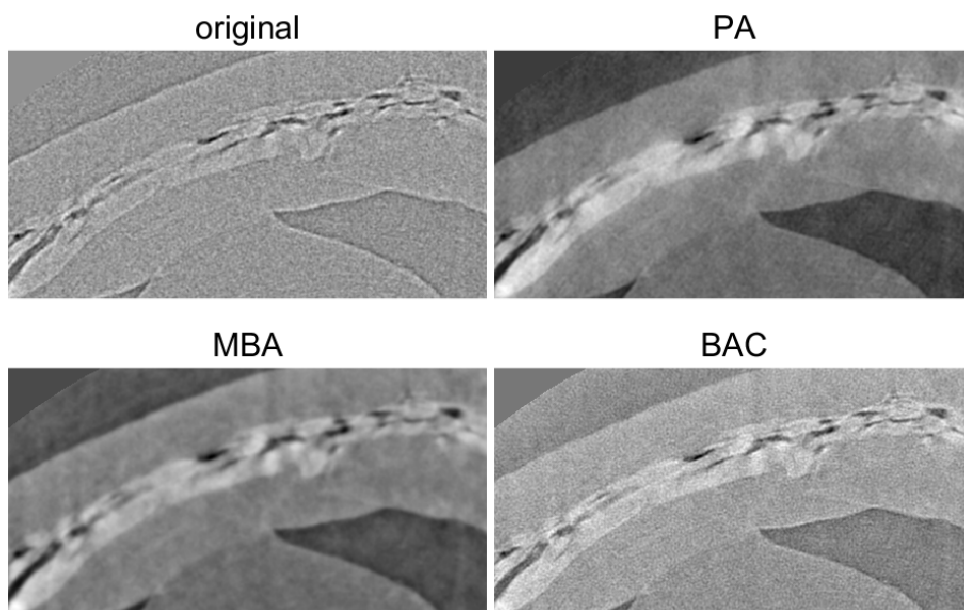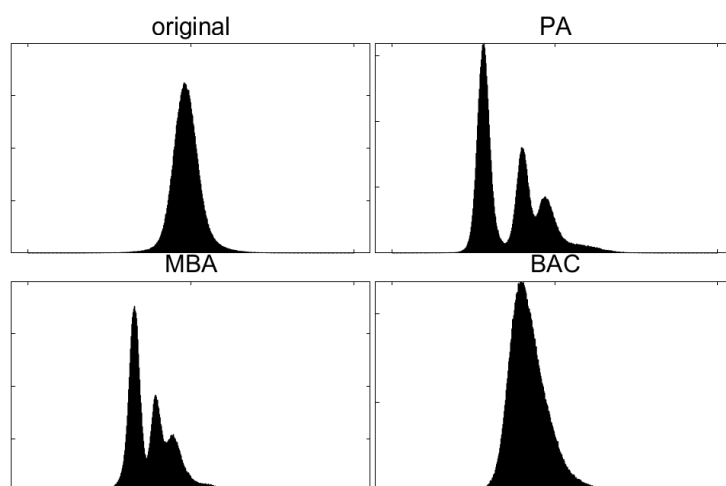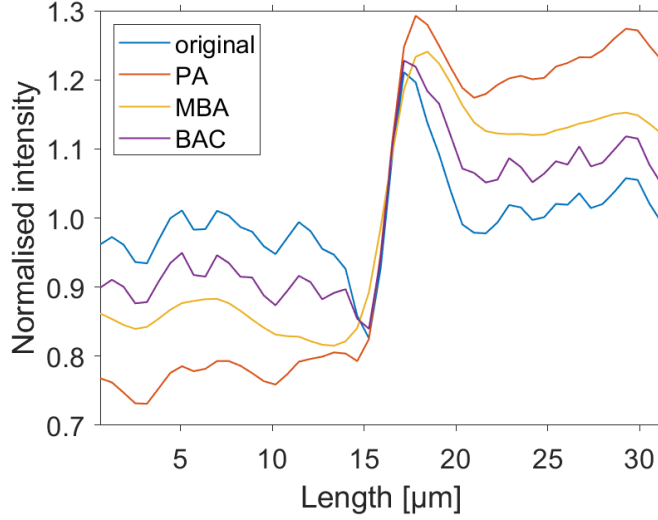
Figure 3.12: Line profiles in CT slices of PEDT with different phase retrieval algorithms (Paganin algorithm – PA, Modified Bronnikov algorithm – MBA, Bronnikov aided correction – BAC).

3.3. Optimisation of measurement parameters for PBI with nano3DX

When performing absorption CT with nano3DX, the setting is rather simple – a detector is placed close to a sample, a sample is centered so that the feature of interest is in the field of view for all angles, and the exposure time is set so there is enough signal on the detector. The minimal signal required for the data obtained with sufficient quality is defined by the manufacturer of the CT machine. However, an optimal signal needed for PBI is not defined. This study was designed to verify whether increasing exposure time or adjusting the sample–detector distance has a positive, if any, effect on quality of PBI data. Since PBI data are usually processed with phase retrieval, the main figures of merit are the SNR_{gain} and $C_{\text{ABS, gain}}$ (Sec. 2.3).

Methodology

The light-element composite made of polyethylene matrix reinforced with carbon fibres (CFRP) was used for the testing (the same sample as in Sec. 3.1.1). Two kinds of experiments with nano3DX with the CCD camera were performed. The CT scans were performed at two different SDDs (2 mm and 5 mm) with three exposure times each (9 s corresponding to the signal defined by manufacturer, 12 s and 15 s) (Tab. 3.3a). Shorter exposure times were avoided to exclude low signal data. Longer exposure times were not tested since they are used only sporadically resulting in long measurement times. All measurements were performed with bin 2, LPS 0.54 μm and 800 projections. The SDD 2 mm corresponds to maximum SDD which is allowed to avoid geometrical unsharpness in this case [7]. The second SDD, 5 mm, was longer than this one, relying on the premise that advantages of bigger phase contrast outweigh or compensate the loss of resolution.

To further study limits of the machine's settings, the second set of measurements was proposed with only projections taken at distances 2 mm, 5 mm and 8 mm and exposure

times 6 s (lower signal then recommended), 9 s, 12 s, 15 s and 25 s (longer exposure time would result in saturation of the detector) (Tab. 3.3b). The measurements were performed with bin 2, LPS 0.54 μm.

The Paganin phase retrieval was applied with δ/β ratio 780, the value for polyethylene [7, 9]. All slices had been normalised before image evaluation unless stated otherwise. Applied image evaluation parameters are listed in Sec. 2.3. The evaluated areas are highlighted in corresponding CT slices and projections in Fig. 3.13.

		Exposure time [s]		
		9	12	15
SDD [mm]	2	✓	✓	✓
	5	✓	✓	✓

(a) CT scans

		Exposure time [s]			
		6	9	15	25
	2	✓	✓	✓	✓
SDD [mm]	5	✓	✓	✓	✓
	8	✓	✓	✓	✓

(b) Projections

Table 3.3: Experiments designed to optimize PBI with nano3DX.

(a)   (b)
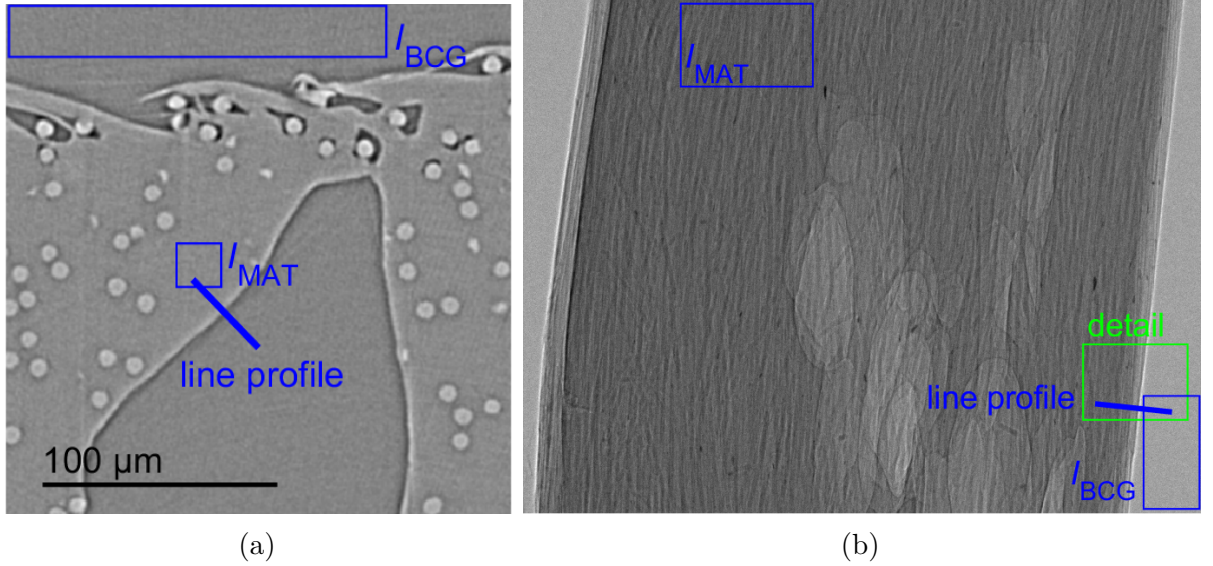
Figure 3.13: Image evaluation regions of measurements of CFRP, a) CT slice, b) projection.

Results

In the data from CT scans, which were obtained in a relatively small range of SDD and exposure times, there is no big visual difference either in original nor in phase retrieved slices. In projections data, a higher amount of edge enhancement is visibly present at higher SDDs, and the decreasing amount of noise with increasing exposure time is noticeable. This results in SNR increasing with exposure time. However, SNR_{gain} is higher for lower exposure times, which suggests that with use of phase retrieval, it is not necessary to increase exposure time in PBI measurement to get better results. It may be possible to use a little bit lower exposure time than necessary in cases, where the radiation damage could be a problem.

C_{ABS} or $C_{\text{ABS, gain}}$ does not change significantly within a small range of exposure times. For higher exposure times like $25\,\text{s}$, the contrast significantly drops. It is understandable from the examination of histograms of individual projections. Peaks in histograms of non-normalised projections are shifted to the right with increasing exposure time. From some point, the response of the detector to incoming X-rays is no longer linear, and the contrast between the sample and background decreases. It also means that peaks of a sample and background are closer to each other in histograms of normalised projections.

SNR_{gain} is, in general, bigger for lower SDDs. It is the opposite trend than in CT slices. $C_{\text{ABS, gain}}$, on the other hand, is lower for lower SDDs. C_{ABS} does not depend on SDD very much. Nevertheless, with increasing SDD, the data are more blurred due to finite focal spot size, which is usually the more important issue.

Summary

The results of this study suggest that there is no substantial change in the quality of phase retrieved PBI data if a user varies the experimental conditions in a small range, which is reasonable for the actual measurement. It is possible to increase the exposure time to get data with higher SNR, but one has to avoid using non-linear part of the detector's sensitivity, and the contrast and SNR gain is not very significant. For nano3DX, this means keeping the exposure time as recommended by the manufacturer. It is acceptable to increase the maximum allowed SDD restricted by geometrical unsharpness to obtain more phase contrast, but only about a small amount (a few millimetres).

4. Applications

In this chapter, selection of CT measurements of various kinds of biomaterials is reported. Specifications regarding applied CT methods and/or staining are emphasized. Only a limited number of images and results is included in this doctoral thesis summary.

4.1. Scaffolds with cells

In tissue engineering, scaffolds are used for healing of bone or cartilage defects. These porous, biodegradable structures are implanted into the damaged region. The surrounding tissue will grow through the scaffold, and it transforms into the tissue itself, serving as a reinforcement. This procedure is supposed to be less invasive for the patient since the number of surgical interventions should be reduced. Imaging of scaffolds by X-ray computed tomography brings 3D information about the success of creating scaffold structures and seeding them with cells. It can be used for verification of the scaffold's preparation and cell's behaviour within the scaffold, its adhesion and proliferation.

CT imaging of scaffolds with cells, distinguishing of cells from the scaffold and their characterization are still the unsolved issues. Many studies have been made in this field, both at synchrotrons ([11–18]) and with laboratory X-ray sources [19–22]. There are various cases from both microCT and medCT categories. Some authors use staining for increased contrast of the cells and/or scaffold.

Here, two different types of CT studies are presented. Imaging of individual cells at very high resolution (Sec. 4.1.1) allows to study in detail the shape and contact area of a single cell. Using worse resolution, but a larger field of view (Sec. 4.1.2), one can observe 3D morphology of a region containing a lot of cells. It is possible to determine characterictics such as volume fraction, contact area, wall thickness, etc., which subsequently helps to understand behavior of the cells and their interaction with scaffold.

4.1.1. High resolution: single cell

This feasibility study shows nCT imaging of an individual cell within a collagen scaffold. The measurement was made at the University of Jyväskylä at Erasmus stay in spring 2018. Phase retrieval is used to enhance the contrast of cell and its nucleus and scaffold.

Sample preparation and measurement

A collagen scaffold seeded with mesenchymal stem cells from human lipoaspirate cultivated for six days and stained with tannic acid and uranyl acetate (TaUA) was measured with Zeiss Xradia nanoXCT-100 described in Sec. 2.1. The sample was glued to a needle, and the very top of the sample was scanned. The CT machine was set in the absorption

mode with a large field of view (LFoV). The binning 2 was used to reach the linear voxel size 130 nm. With 541 projections and exposure time of 10 s the scan lasted about 1.5 h. For larger scanning times (several days), the sample was damaged, probably due to a high X-ray dose. Paganin phase retrieval algorithm was applied to X-ray projections to enhance data quality.

Results

The TaUA staining was more selective for the scaffold than for the cell (Fig. 4.1a). However, the grey value distribution in the reconstructed data has Gaussian-like shape, which makes segmentation of the scaffold and the cell difficult. As it was demonstrated before, application of the phase retrieval algorithm (Fig. 4.1b) led to data with increased contrast and different grey values distribution in histogram. From phase-retrieved data, the cell and scaffold were segmented and visualised in 3D space. Moreover, the nucleus of the cell is distinguishable in the CT slice (Fig. 4.1b).

Summary

This study shows the capability of the laboratory nCT device to image the cell within the scaffold. TaUA staining and phase contrast enhancement are used to create a visible contrast between both structures. Therefore it was possible to segment them and visualize in 3D. Such a procedure can be useful for imaging of soft materials, where structures with very similar X-ray absorption are to be imaged and analysed.
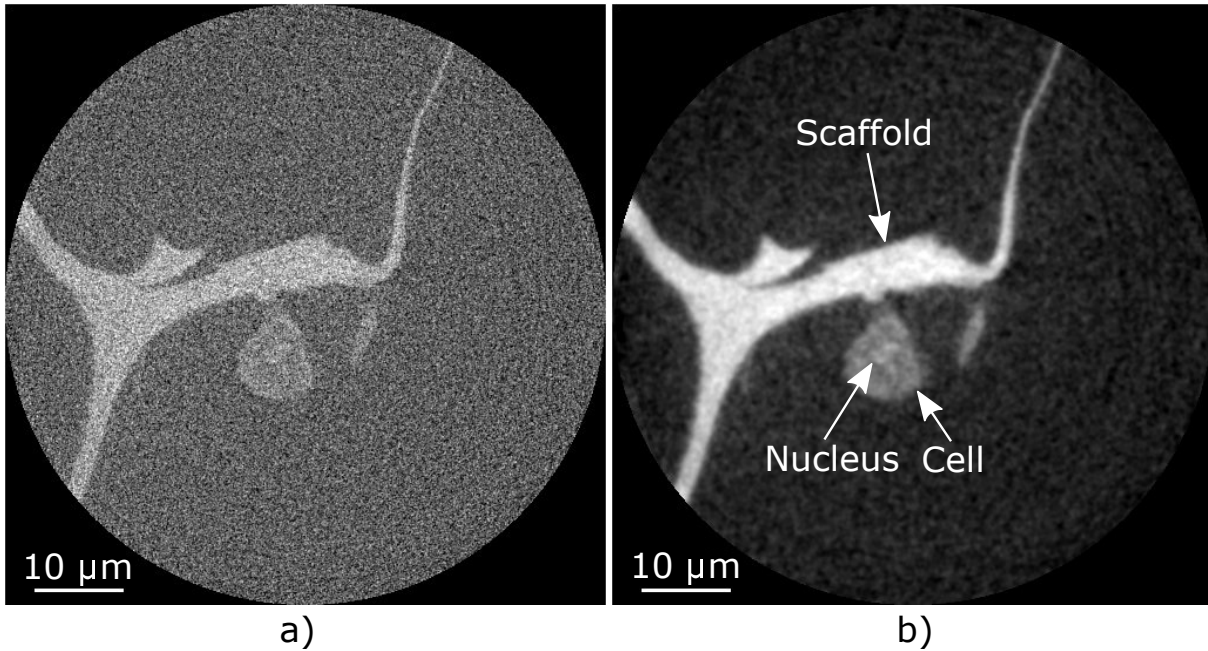

Figure 4.1: CT slice of the scaffold with a cell; a) original reconstruction (absorption contrast), b) phase retrieved CT slice (phase contrast).

4.1.2. Large field of view: statistical evaluation

This study shows sub-micronCT analysis of scaffolds with cells with CT device nano3DX. In comparison to the previous study, the goal here is to evaluate a bigger region with higher amount of cells. The complete analysis of this sample was published in [23].

Sample preparation and measurement

Collagen porous scaffold seeded with rabbit mesenchymal stem cells (MSC) was stained with OsO_4. The CT measurement was performed with the RIGAKU nano3DX device with a CCD camera with the following parameters: Cu target, field of view $0.7\,mm \times 0.9\,mm$, binning 2, linear voxel size $0.54\,\mu m$, 800 projections, exposure time $10\,s$. The projections were filtered using nonlocal means denoising filter. Movement artefacts were reduced with a custom-developed movement correction technique based on the phase correlation. Paganin phase retrieval was used to enhance the contrast between cells and scaffold. More details in [23].

Results

Prior to the CT measurements, the scanning electron microscopy with an energy dispersive X-ray spectroscopy was used to verify the presence and positions of MSCs. Elemental distribution of osmium showed an increased concentration on the cell's surface. Phase retrieval further increased contrast between cells and scaffold in CT data, so it was possible to segment the cells based on different grey values.

The 3D render shows the distribution of cells throughout the scaffold (Fig. 4.2). By visual inspection, it is possible to observe the shape and distribution of cells. Knowledge of cell's proliferation is especially useful when samples with different cultivation times are compared.
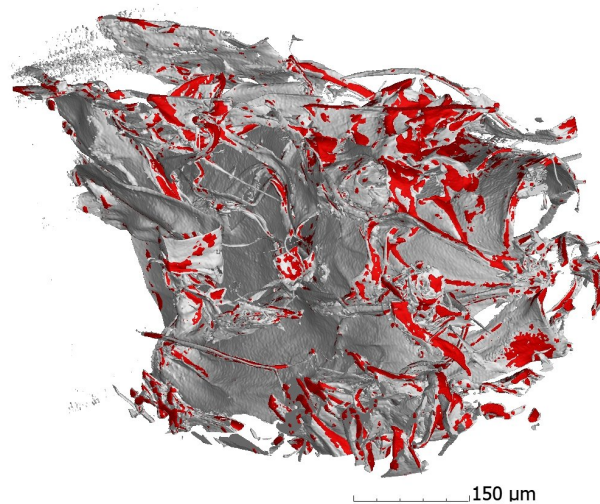

150 µm

Figure 4.2: 3D rendering of a collagen scaffold with seeded MSC cells labeled in red colour.

4.2. Porosity of open foam structures

Porosity is one of the most significant properties when describing individual samples. It is defined as a ratio of air volume and total sample volume. There are many methods for the determination of porosity, either in 2D or 3D – Archimedes method, scanning electron microscopy, mercury porosimetry, gas pycnometry etc. [24] Among other techniques, X-ray computed tomography is nondestructive and 3D, but limited in resolution [25, 26]. The best method is individual for each application, and it is often advantageous to use more complementary techniques.

To obtain quantitative information of single, enclosed cavities (enclosed porosity, Fig. 4.3a) in CT data is a prevalent task in the industry. Each pore is a separate volume surrounded by the material. Information of interest includes a list of pores with their sizes, volumes and positions, and morphological information about their distribution within the bulk of the sample. In tissue engineering, the more common situation is when the pores are interconnected within the structure (open porosity, Fig. 4.3b). The structure itself is more like a network of thin walls rather than bulk filled with material. It is a case of many biomaterial applications like foams and scaffolds. In this case, the software first has to divide the pore space into single pores. Subsequently, additional information about pore space can be obtained such as distribution, quantification and statistics of the areas between the pores and the pore network.

To get quantitative information about open porosity in samples scanned with CT, different software offers various approaches. A comparison of different software for open porosity analysis of CT data was presented at the CEITEC PHD retreat II. conference [27]. The analysis of this type of samples in VGStudio MAX was published in [28]. Both studies were performed on a sample of hydroxyapatite foam measured with GE phoenix v|tome|x L240 (Sec. 2.1).
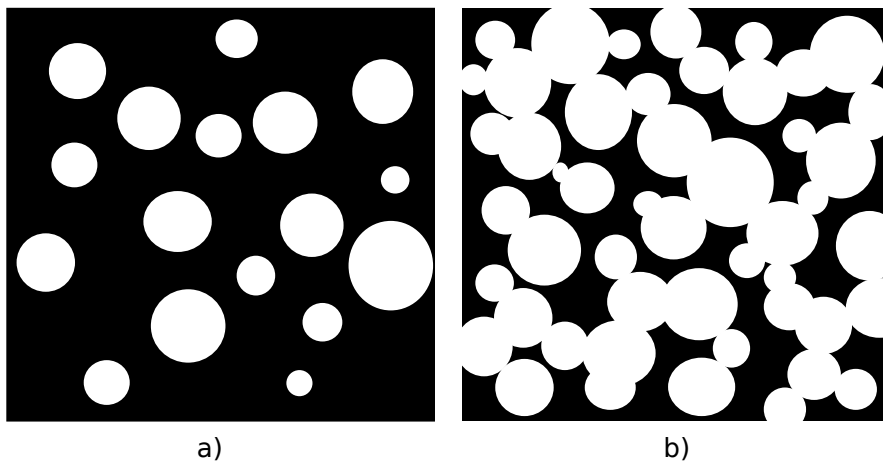

a)   b)

Figure 4.3: Schematic drawing of a) enclosed and b) open porosity. In enclosed porosity, each pore occurs separately. Open porosity is characterized by interconnected pores creating one pore network.

4.3. Correlation of CT data with 2D imaging techniques

All imaging methods have their advantages and disadvantages, and all offer examination from some point of view. For a complete description of a sample, it is often advantageous to combine them via some multi-disciplinary approach. For biological specimens, many authors combine CT measurements with optical microscopy images of histological sections [29, 30] or transmission electron microscopy [31]. In material science, and also tissue engineering, scanning electron microscopy is used [16].

CT can also be combined with other 3D methods. In medicine, CT is combined with positron emission tomography [32, 33], or with magnetic resonance imaging [34, 35] since those methods are more sensitive to different kinds of tissues and they may help with artefact removal. Serial sectioning by focused ion beam with elemental or chemical mapping by energy dispersive X-ray spectroscopy or electron backscatter diffraction is used to describe CT data qualitatively [36–38]. Large-scale CT images can be supplemented with CT images focused on some region of interest imaged with higher resolution [39].

In studies presented in this section, CT data do not give information about which grey values correspond to which element or material inside the sample. The contrast is based only on different properties of different parts of a sample in the X-ray region. 2D optical and electron microscopy are used as a reference for the interpretation of CT data. Moreover, in Sec. 4.3.1, a sample holder for easier correlation of SEM and CT data is presented.

4.3.1. nCT, SEM and LM of scaffolds

The collagen scaffold structure was observed using the nCT device RIGAKU nano3DX and the scanning electron microscope (SEM) Tescan MIRA3. As a supplementary method, light microscopy (LM) was used. Since all machines have different geometrical arrangements, a sample holder compatible with nCT and SEM was designed. To locate precisely the same regions of interest in all methods, a test of markers placed on the sample was performed.

The study was presented by the author of the thesis at XRM 2018 conference and published in [40], titled "Correlation of X-ray Computed Nanotomography and Scanning Electron Microscopy Imaging of Collagen Scaffolds".

4.3.2. CT, 3D EDS analysis and LM of limestone

Although this experiment does not refer to a biomaterial, it is a good example of correlation of CT data with other methods. Combination of several methods on limestone sample helps with identification of materials within the sample. The study was published by the author of the thesis in [41], titled "Characterization of inner structure of limestone by X-ray computed sub-micron tomography".

Abstract

"Limestones are fundamental industrial and building materials. Sparry calcite as a principal petrographic component of limestones can contain fluid inclusions. A certain amount

4. APPLICATIONS

of fluid inclusions directly influences decrepitation which plays an important role in decarbonisation processes.

In this paper, a limestone with a high content of fluid inclusions and carbon was investigated. Presence of chlorine and alcalic elements was confirmed with microthermometry, mineralogical and chemical analyses. X-ray computed tomography with submicron resolution (CT) was applied to obtain a 3D distribution of cavities. CT data were correlated with some light microscopy images and also with the same sample's tomography data which were gathered using the 3D X-ray energy dispersive spectroscopy (3D EDS) by a scanning electron microscope equipped with a focused ion beam (FIB-SEM). The latter further determined dolomites and metals in the CT data of limestone." [41]

Conclusion

The topic of the thesis reflects the current need of scientists to have a 3D, nondestructive, high-resolution imaging method of investigation of soft samples to complement established 2D microscopy techniques. Although the CT was originally developed for clinical purpose, the straightforward application on smaller samples and with higher resolution does not reflect the small X-ray absorption of soft tissues and their inclination to movement. Therefore in many cases, special measurement protocols and methods or specific post-processing procedures have to be adapted to be able to fully exploit all advantages of X-ray computed tomography.

One of the challenges is that biomaterials often do not have enough contrast in X-ray region to be measured with sufficient quality by common absorption CT. In such cases, staining of samples or phase contrast imaging methods have to be used. The latter is the method widely studied and exploited in the thesis. Propagation-based method of phase contrast imaging with laboratory X-ray sources was studied on specific CT devices. A theoretical description of the machines helps to understand its capabilities of PBI and estimate its limitations. Several sets of experiments were performed to test various theoretical statements regarding phase contrast theory and geometrical arrangement. Application of phase retrieval on CT data was shown as a useful tool for enhancing data quality. A graphical user interface for implementing and testing of phase retrieval algorithms was designed.

To establish the CT technique as a standard examination tool, it has to be put within the framework of methods already commonly used in practice and the advantages have to be demonstrated on specific examples. Examples of image processing of CT data from various machines were shown, including morphology characteristics, volumetric analysis, and porosity analysis. Supporting 2D examination methods may be used as a qualitative methods to determine the sample's composition, whereas CT observes the whole sample quantitatively. To demonstrate that such a correlation is possible and advantageous, two case-studies presented a combination of CT, light microscopy, scanning electron microscopy and 3D energy dispersive X-ray spectroscopy. A sample holder which fits both into CT and SEM machines was designed to help with a mutual correlation of data.

The particular contribution of this work is the extension of expertise in phase contrast imaging within the Laboratory of X-ray micro and nano computed tomography at CEITEC BUT. Implementation of this method on specific topics from material research extends the possibilities of characterisation of materials, primarily in the field of soft materials. In general, this thesis contributes to the establishment of an X-ray computed tomography technique as a common tool for 3D imaging and analysis of biomaterials. The most important results presented in this work are published by the author in impacted journals [7, 40, 41] and international conferences [27, 42] so the scientific community can benefit from the findings.

CONCLUSION

References

[1] SCHINDELIN, J., I. ARGANDA-CARRERAS, E. FRISE, V. KAYNIG, M. LON-GAIR, T. PIETZSCH, S. PREIBISCH, C. RUEDEN, S. SAALFELD, B. SCHMID, J.-Y. TINEVEZ, D. J. WHITE, V. HARTENSTEIN, K. ELICEIRI, P. TOMAN-CAK and A. CARDONA. Fiji: an open-source platform for biological-image analysis. *Nature Methods*. 2012, vol. 9, no. 7, pp. 676–682. ISSN 15487091. Available from: doi:10.1038/nmeth.2019.

[2] RUEDEN, C. T., J. SCHINDELIN, M. C. HINER, B. E. DEZONIA, A. E. WAL-TER, E. T. ARENA and K. W. ELICEIRI. ImageJ2: ImageJ for the next generation of scientific image data. *BMC Bioinformatics*. 2017, vol. 18, no. 1, pp. 529. ISSN 14712105. Available from: doi:10.1186/s12859-017-1934-z.

[3] *MATLAB*. [online]. USA: The MathWorks, Inc. Available from: `https://se.mathworks.com/products/matlab.html`.

[4] *VGStudio MAX*. [online]. Germany: Volume Graphics GmbH. Available from: `https://www.volumegraphics.com/en/products/vgstudio-max.html`.

[5] *MAVI - Modular Algorithms for Volume Images*. [online]. Germany: Fraunhofer Institute fo Industrial Mathematics. Available from: `https://www.itwm.fraunhofer.de/en/departments/bv/products-and-services/mavi.html`.

[6] BRUN, F., L. MANCINI, P. KASAE, S. FAVRETTO, D. DREOSSI and G. TROMBA. Pore3D: A software library for quantitative analysis of porous media. *Nuclear Instruments and Methods in Physics Research, Section A: Accelerators, Spectrometers, Detectors and Associated Equipment*. 2010, vol. 615, no. 3, pp. 326–332. ISSN 01689002. Available from: doi:10.1016/j.nima.2010.02.063.

[7] KALASOVÁ, D., T. ZIKMUND, L. PÍNA, Y. TAKEDA, M. HORVÁTH, K. OMOTE and J. KAISER. Characterization of a laboratory-based X-ray computed nanotomography system for propagation-based method of phase contrast imaging. *IEEE Transactions on Instrumentation and Measurement*. 2019. Available from: doi:10.1109/TIM.2019.2910338.

[8] POLUDNIOWSKI, G., G. LANDRY, F. DEBLOIS, P. M. EVANS and F. VER-HAEGEN. SpekCalc : a program to calculate photon spectra from tungsten anode x-ray tubes. *Physics in Medicine and Biology*. 2009, vol. 54, no. 19. ISSN 0031-9155. Available from: doi:10.1088/0031-9155/54/19/N01.

[9] *X-ray complex refraction coefficient*. [online]. [Visited on 2016-1-7]. Available from: `http://ts-imaging.net/Services/Simple/ICUtilXdata.aspx`.

REFERENCES

[10] TÖPPERWIEN, M., M. KRENKEL, F. QUADE and T. SALDITT. Laboratory-based x-ray phase-contrast tomography enables 3D virtual histology. In: *Advances in Laboratory-based X-Ray Sources, Optics, and Applications V*. 2016. Available from: doi:10.1117/12.2246460.

[11] THURNER, P., B. MÜLLER, F. BECKMANN, T. WEITKAMP, C. RAU, R. MÜLLER, J. A. HUBBELL and U. SENNHAUSER. Tomography studies of human foreskin fibroblasts on polymer yarns. *Nuclear Instruments and Methods in Physics Research Section B: Beam Interactions with Materials and Atoms*. 2003, vol. 200, pp. 397–405. ISSN 0168583X. Available from: doi:10.1016/S0168-583X(02)01729-9.

[12] THURNER, P., B. MÜLLER, U. SENNHAUSER, J. HUBBELL and R. MÜLLER. Tomography studies of biological cells on polymer scaffolds. *Journal of Physics: Condensed Matter*. 2004, vol. 16, no. 33, pp. S3499–S3510. ISSN 0953-8984. Available from: doi:10.1088/0953-8984/16/33/011.

[13] TORRENTE, Y., M. GAVINA, M. BELICCHI, F. FIORI, V. KOMLEV, N. BRESOLIN and F. RUSTICHELLI. High-resolution X-ray microtomography for three-dimensional visualization of human stem cell muscle homing. *FEBS Letters*. 2006, vol. 580, no. 24, pp. 5759–5764. ISSN 00145793. Available from: doi:10.1016/j.febslet.2006.09.031.

[14] ALBERTINI, G., A. GIULIANI, V. KOMLEV, F. MORONCINI, A. PUGNALONI, G. PENNESI, M. BELICCHI, C. RUBINI, F. RUSTICHELLI, R. TASSO and Y. TORRENTE. Organization of Extracellular Matrix Fibers Within Polyglycolic Acid–Polylactic Acid Scaffolds Analyzed Using X-Ray Synchrotron-Radiation Phase-Contrast Micro Computed Tomography. *Tissue Engineering Part C: Methods*. 2009, vol. 15, no. 3, pp. 403–411. ISSN 1937-3384. Available from: doi:10.1089/ten.tec.2008.0270.

[15] ZEHBE, R., J. GOEBBELS, Y. IBOLD, U. GROSS and H. SCHUBERT. Three-dimensional visualization of in vitro cultivated chondrocytes inside porous gelatine scaffolds: A tomographic approach. *Acta Biomaterialia*. 2010, vol. 6, no. 6, pp. 2097–2107. ISSN 17427061. Available from: doi:10.1016/j.actbio.2009.11.020.

[16] THIMM, B. W., S. HOFMANN, P. SCHNEIDER, R. CARRETTA and R. MÜLLER. Imaging of Cellular Spread on a Three-Dimensional Scaffold by Means of a Novel Cell-Labeling Technique for High-Resolution Computed Tomography. *Tissue Engineering Part C: Methods*. 2012, vol. 18, no. 3, pp. 167–175. ISSN 1937-3384. Available from: doi:10.1089/ten.tec.2011.0262.

[17] CEDOLA, A., G. CAMPI, D. PELLICCIA, I. BUKREEVA, M. FRATINI, M. BURGHAMMER, L. RIGON, F. ARFELLI, R. CHANG CHEN, D. DREOSSI, N. SODINI, S. MOHAMMADI, G. TROMBA, R. CANCEDDA and M. MASTRO-GIACOMO. Three dimensional visualization of engineered bone and soft tissue by combined x-ray micro-diffraction and phase contrast tomography. *Physics in Medicine and Biology*. 2014, vol. 59, no. 1, pp. 189–201. ISSN 0031-9155. Available from: doi:10.1088/0031-9155/59/1/189.

[18] GIULIANI, A., F. MORONCINI, S. MAZZONI, M. L. C. BELICCHI, C. VILLA, S. ERRATICO, E. COLOMBO, F. CALCATERRA, L. BRAMBILLA, Y. TORRENTE, G. ALBERTINI and S. DELLA BELLA. Polyglycolic Acid–Polylactic Acid Scaffold Response to Different Progenitor Cell In Vitro Cultures: A Demonstrative and Comparative X-Ray Synchrotron Radiation Phase-Contrast Microtomography

Study. *Tissue Engineering Part C: Methods*. 2014, vol. 20, no. 4, pp. 308–316. ISSN 1937-3384. Available from: doi:10.1089/ten.tec.2013.0213.

[19] CHAMIEH, F., A.-M. COLLIGNON, B. R. COYAC, J. LESIEUR, S. RIBES, J. SADOINE, A. LLORENS, A. NICOLETTI, D. LETOURNEUR, M.-L. COLOMBIER, S. N. NAZHAT, P. BOUCHARD, C. CHAUSSAIN and G. Y. ROCHEFORT. Accelerated craniofacial bone regeneration through dense collagen gel scaffolds seeded with dental pulp stem cells. *Scientific Reports*. 2016, vol. 6, no. 1, pp. 38814. Available from: doi:10.1038/srep38814.

[20] SHEPHERD, D. V., J. H. SHEPHERD, S. M. BEST and R. E. CAMERON. 3D imaging of cells in scaffolds: direct labelling for micro CT. *Journal of Materials Science: Materials in Medicine*. 2018, vol. 29, no. 6, pp. 86. ISSN 0957-4530. Available from: doi:10.1007/s10856-018-6089-6.

[21] PAPANTONIOU, I., M. SONNAERT, L. GERIS, F. P. LUYTEN, J. SCHROOTEN and G. KERCKHOFS. Three-Dimensional Characterization of Tissue-Engineered Constructs by Contrast-Enhanced Nanofocus Computed Tomography. *Tissue Engineering Part C: Methods*. 2014, vol. 20, no. 3, pp. 177–187. ISSN 1937-3384. Available from: doi:10.1089/ten.tec.2013.0041.

[22] BRADLEY, R. S., I. K. ROBINSON and M. YUSUF. 3D X-Ray Nanotomography of Cells Grown on Electrospun Scaffolds. *Macromolecular Bioscience*. 2017, vol. 17, no. 2, pp. 1600236. ISSN 16165187. Available from: doi:10.1002/mabi.201600236.

[23] VOJTOVÁ, L., T. ZIKMUND, V. PAVLIŇÁKOVÁ, J. ŠALPLACHTA, D. KALASOVÁ, E. PROSECKÁ, J. BRTNÍKOVÁ, J. ŽÍDEK, D. PAVLIŇÁK and J. KAISER. The 3D imaging of mesenchymal stem cells on porous scaffolds using high-contrasted x-ray computed nanotomography. *Journal of Microscopy*. 2019, vol. 273, no. 3, pp. 169–177. ISSN 00222720. Available from: doi:10.1111/jmi.12771.

[24] ANOVITZ, L. M. and D. R. COLE. Characterization and Analysis of Porosity and Pore Structures. *Reviews in Mineralogy and Geochemistry*. 2015, vol. 80, no. 1, pp. 61–164. ISSN 1529-6466. Available from: doi:10.2138/rmg.2015.80.04.

[25] HO, S. T. and D. W. HUTMACHER. A comparison of micro CT with other techniques used in the characterization of scaffolds. *Biomaterials*. 2006, vol. 27, no. 8. ISSN 01429612. Available from: doi:10.1016/j.biomaterials.2005.08.035.

[26] ZOU, Y. and J. MALZBENDER. Development and optimization of porosity measurement techniques. *Ceramics International*. 2016, vol. 42, no. 2, pp. 2861–2870. ISSN 02728842. Available from: doi:10.1016/j.ceramint.2015.11.015.

[27] KALASOVÁ, D., T. ZIKMUND and J. KAISER. Computed Tomography for Inspection of Inner Structure of Materials. In: *CEITEC PhD Retreat II, Telč 20-21 April 2017 - Book of Abstracts*. Masaryk University, 2017. ISBN 978-80-210-8550-3.

[28] STASTNY, P., Z. CHLUP, D. KALASOVA, T. ZIKMUND, J. KAISER and M. TRUNEC. Epoxy-based gelcasting of machinable hydroxyapatite foams for medical applications. *Journal of the American Ceramic Society*. 2018, vol. 101, no. 8, pp. 3317–3327. ISSN 00027820. Available from: doi:10.1111/jace.15523.

REFERENCES

[29] WALTON, L. A., R. S. BRADLEY, P. J. WITHERS, V. L. NEWTON, R. E. WATSON, C. AUSTIN and M. J. SHERRATT. Morphological characterisation of unstained and intact tissue micro-architecture by X-ray computed micro- and nanotomography. *Scientific Reports.* 2015, vol. 6, no. 6. ISSN 20452322. Available from: doi:10.1038/srep10074.

[30] PALLUA, J. D., V. KUHN, R. PÖDER, A. F. PALLUA, K. PFALLER, W. RECHEIS and A. K. PALLUA. Application of micro-computed tomography to microstructure studies of the medicinal fungus Hericium coralloides. *Mycologia.* 2015, vol. 107, no. 1, pp. 227–238. ISSN 0027-5514. Available from: doi:10.3852/14-188.

[31] PARLANTI, P., V. CAPPELLO, F. BRUN, G. TROMBA, R. RIGOLIO, I. TONAZZINI, M. CECCHINI, V. PIAZZA and M. GEMMI. Size and specimen-dependent strategy for x-ray micro-ct and tem correlative analysis of nervous system samples. *Scientific Reports.* 2017, vol. 7, no. 1. ISSN 20452322. Available from: doi:10.1038/s41598-017-02998-1.

[32] BEYER, T., D. TOWNSEND, T. BRUN, P. KINAHAN, M. CHARRON, R. RODDY, J. JERIN, J. YOUNG, L. BYARS and R. NUTT. A combined PET/CT scanner for clinical oncology. *Journal of nuclear medicine : official publication, Society of Nuclear Medicine.* 2000, vol. 41, no. 8, pp. 1369–1379. ISSN 0161-5505.

[33] ERGONUL, A. G., T. I. AKCAM, A. ÖZDIL, K. TURHAN, A. CAKAN and U. CAGIRICI. Diagnostic value of 18F-FDG-PET/CT in benign lung diseases. *Kardiochirurgia i Torakochirurgia Polska.* 2018, vol. 6, no. 6, pp. 1–4. ISSN 17315530. Available from: doi:10.5114/kitp.2018.74667.

[34] LEE, Y. S., J. K. SEON, V. I. SHIN, G. H. KIM and M. JEON. Anatomical evaluation of CT-MRI combined femoral model. *BioMedical Engineering Online.* 2008, vol. 6, no. 6, pp. 6. ISSN 1475925X. Available from: doi:10.1186/1475-925X-7-6.

[35] BASHA, M. A. A., A. F. AHMED, S. M. SHEHATA, D. A. E. A. EL SAMMAK, E. H. ABDELBARY, A. A. OBAYA, T. FATHY, H. Y. YOUSEF and M. Z. ALAZZAZY. Does a combined CT and MRI protocol enhance the diagnostic efficacy of LI-RADS in the categorization of hepatic observations? A prospective comparative study. *European Radiology.* 2018, vol. 6, no. 6, pp. 2592–2603. ISSN 0938-7994. Available from: doi:10.1007/s00330-017-5232-y.

[36] ASAIZUMI, M., T. KATO, T. KUGA, N. OODE, T. ODA, T. SAKURADA, K. THOMSON, T. TABARA and R. I. KARLINSEY. Submicron X-Ray Computed Tomography of Human Dentin Treated with Topical Fluoride Modalities. *EC Dental Science.* 2016, no. 5.2, pp. 992–1017.

[37] BURNETT, T. L., S. A. MCDONALD, A. GHOLINIA, R. GEURTS, M. JANUS, T. SLATER, S. J. HAIGH, C. ORNEK, F. ALMUAILI, D. L. ENGELBERG, G. E. THOMPSON and P. J. WITHERS. Correlative tomography. *Scientific Reports.* 2014, vol. 6, no. 6. ISSN 20452322. Available from: doi:10.1038/srep04711.

[38] DE BOEVER, W., H. DERLUYN, D. VAN LOO, L. VAN HOOREBEKE and V. CNUDDE. Data-fusion of high resolution X-ray CT, SEM and EDS for 3D and pseudo-3D chemical and structural characterization of sandstone. *Micron.* 2015, vol. 74, pp. 15–21. ISSN 09684328. Available from: doi:10.1016/j.micron.2015.04.003.

[39] CHAURAND, P., W. LIU, D. BORSCHNECK, C. LEVARD, M. AUFFAN, E. PAUL, B. COLLIN, I. KIEFFER, S. LANONE, J. ROSE and J. PERRIN. Multi-scale X-ray computed tomography to detect and localize metal-based nanomaterials in lung tissues of in vivo exposed mice. *Scientific Reports*. 2018, vol. 8, no. 1. ISSN 20452322. Available from: doi:10.1038/s41598-018-21862-4.

[40] KALASOVÁ, D., V. PAVLIŇÁKOVÁ, T. ZIKMUND, L. VOJTOVÁ and J. KAISER. Correlation of X-ray Computed Nanotomography and Scanning Electron Microscopy Imaging of Collagen Scaffolds. *Microscopy and Microanalysis*. 2018, vol. 24, no. S2, pp. 104–105. ISSN 1431-9276. Available from: doi:10.1017/S1431927618012904.

[41] KALASOVÁ, D., K. DVOŘÁK, M. SLOBODNÍK, D. VŠIANSKÝ, T. ZIKMUND, J. DLUHOŠ, R. VÁŇA, J. BUREŠ and J. KAISER. Characterization of inner structure of limestone by X-ray computed sub-micron tomography. *Construction and Building Materials*. 2018, vol. 6, no. 6, pp. 693–700. ISSN 09500618. Available from: doi:10.1016/j.conbuildmat.2018.04.142.

[42] KALASOVÁ, D., J. MAŠEK, T. ZIKMUND, P. SPURNÝ, J. HALODA, R. BURGET and J. KAISER. Segmentation of Multi-Phase Object Applying Trainable Segmentation. *e-Journal of Nondestructive Testing*. 2017, vol. 2017. ISSN 1435-4934.